Water Research 112 (2017) pp 185-194. DOI: 10.1016/j.watres.2017.01.030

How Do Operating Conditions Affect As(III) Removal by Iron Electrocoagulation?

Caroline Delaire*[,†], Susan Amrose[†], Minghui Zhang[†], James Hake[§], Ashok Gadgil[†,‡]

[†] Department of Civil and Environmental Engineering, University of California, Berkeley, California 94720-1710, United States

[§] Department of Chemical and Biomolecular Engineering, University of California, Berkeley, California 94720-1710, United States

[‡] Energy Technologies Area, Lawrence Berkeley National Laboratory, Berkeley, California 94720, United States

* Corresponding author: caroline.delaire@orange.fr

Water Research 112 (2017) pp 185-194. DOI: 10.1016/j.watres.2017.01.030

Abstract

Iron electrocoagulation (Fe-EC) has been shown to effectively remove arsenic from contaminated groundwater at low cost and has the potential to improve access to safe drinking water for millions of people. Understanding how operating conditions, such as the Fe dosage rate and the O_2 recharge rate, affect arsenic removal at different pH values is crucial to maximize the performance of Fe-EC under economic constraints. In this work, we improved upon an existing computational model to investigate the combined effects of pH, Fe dosage rate, and O_2 recharge rate on arsenic removal in Fe-EC. We showed that the impact of the Fe dosage rate strongly depends on pH and on the O_2 recharge rate, which has important practical implications. We identified the process limiting arsenic removal (As(III) oxidation versus As(V) adsorption) at different pH values, which allowed us to interpret the effect of operating conditions on Fe-EC performance. Finally, we assessed the robustness of the trends predicted by the model, which assumes a constant pH, against lab experiments reproducing more realistic conditions where pH is allowed to drift during treatment as a result of equilibration with atmospheric CO_2. Our results provide a nuanced understanding of how operating conditions impact arsenic removal by Fe-EC and can inform decisions regarding the operation of this technology in a range of groundwaters.

Keywords: Arsenic; Iron electrocoagulation; Operating conditions; pH; Computational model; Synthetic Bengal groundwater

TOC Graphic

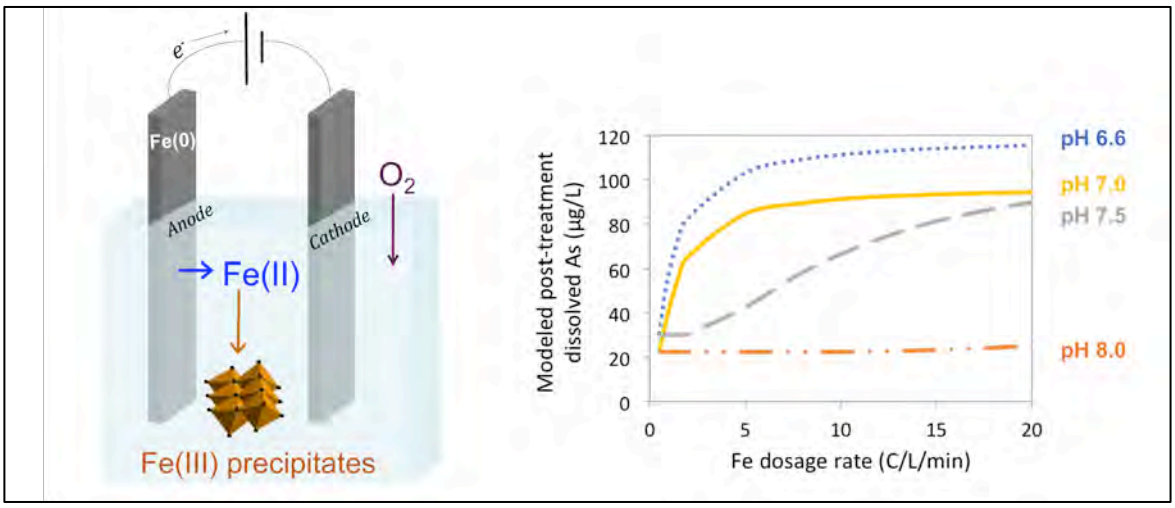

1. Introduction

Millions of people worldwide are exposed to arsenic present in groundwater supplies (Chakraborti et al., 2013; Ravenscroft et al., 2009). In areas where no safer, reliable, and abundant source of drinking water exists, removing arsenic from contaminated groundwater is necessary to protect public health. Iron electrocoagulation (Fe-EC) is a promising arsenic removal technology because it is highly effective, relies on consumables that are available in low-income rural areas, does not involve hazardous chemicals, and produces minimal amounts of sludge (Amrose et al., 2013, 2014; van Genuchten et al., 2012). In Fe-EC, a small voltage is applied between two Fe(0) (usually mild steel) electrodes, leading to the electrolytic dissolution of the anode into aqueous Fe(II). In the presence of dissolved O_2, Fe(II) oxidizes to Fe(III), which is highly insoluble at circumneutral pH and forms Fe(III) (oxyhydr)oxide precipitates with a strong adsorption affinity for arsenic (van Genuchten et al., 2014b, 2012). In addition, reactive intermediates produced upon the oxidation of Fe(II) by O_2, such as Fe(IV), oxidize As(III) to As(V), which is more amenable to adsorption (Hug and Leupin, 2003; Li et al., 2012). The Fe-EC process typically has three phases: 1) electrolysis to produce Fe(II) (in open air and with solution mixing), 2) post-electrolysis mixing to ensure full oxidation of Fe(II) and As(III) as well as arsenic adsorption onto precipitates (in open air), and 3) separation

of arsenic-laden precipitates (e.g., by gravitational settling). Fe-EC is most suitable for operation at the community-scale (Amrose et al., 2014; Holt et al., 2005), as opposed to the household-scale like other Fe-based arsenic removal technologies (e.g., Neumann et al., 2013). Fe-EC has been demonstrated during a 3-month field trial in rural West Bengal, India, to effectively remove arsenic to levels below the World Health Organization (WHO) maximum contaminant limit (MCL) of 10 μg/L, consistently achieving 2.1 ± 1.0 μg/L final total arsenic (Amrose et al., 2014). Before deploying this technology throughout arsenic-affected regions, it is necessary to understand how the performance of Fe-EC can be maximized, under economic constraints, in groundwaters with different chemical compositions.

The performance of Fe-EC can be defined as the arsenic removal efficiency, i.e. as the reduction in arsenic concentration per unit of Fe produced, or per unit of cost. Performance is governed by chemical characteristics of groundwater (e.g., pH and co-occurring ions), certain aspects of the reactor design (e.g., electrode shape and configuration), and EC operating conditions (e.g., Fe dosage rate (Li et al., 2012) and O_2 recharge rate). For example, the amount of Fe required to remove a given concentration of arsenic to below the WHO MCL depends highly on solution pH, which affects both the kinetics of As(III) oxidation (Li et al., 2012) and the affinity of Fe(III) (oxyhydr)oxides for oxyanions (Dixit and Hering, 2003; Gao and Mucci, 2001). Groundwater oxyanions (P, Si) and bivalent cations (Ca, Mg) affect arsenic removal by competing for adsorption sites on EC precipitates (Li et al., 2012; van Genuchten et al., 2014a) and enhancing arsenic uptake (van Genuchten et al., 2014a), respectively. Operating conditions have ambivalent effects on the performance of Fe-EC. For example, increasing the Fe dosage rate (e.g., by increasing the operating current) can reduce the duration of treatment and therefore minimize the costs associated with electricity use for mixing. However, it also leads to the accumulation of Fe(II), which competes with As(III) for reactive intermediates, and can thus increase the amount Fe required to treat groundwater (Li et al., 2012). Inversely, enhancing aeration increases energy costs but may improve arsenic removal by increasing the

rate of Fe(II) oxidation by O_2 and limiting the accumulation of Fe(II). Optimal operating conditions that minimize the cost of treatment are expected to depend on groundwater characteristics, especially on pH, which controls key arsenic removal processes in Fe-EC. In South Asia, the pH of arsenic-contaminated groundwater can vary substantially between 6.4 and 8.4 (British Geological Survey, 2001). Therefore, understanding how operating conditions, such as the Fe dosage rate and the O_2 recharge rate, affect arsenic removal at different pH values is crucial to guide an operator or system designer's decision making.

In this study, we investigated the combined effects of pH, Fe dosage rate, and O_2 recharge rate on arsenic removal by Fe-EC. We improved upon a computational model of Fe-EC previously developed by Li et al. (2012) to predict arsenic removal in a range of groundwater and operating conditions. Specifically, we extended Li's model, which had been developed at pH 7.1, to a realistic pH range (6.6 to 8.1) and incorporated O_2 kinetics. Using the new model, we first identified the process limiting arsenic removal (As(III) oxidation versus As(V) adsorption) at different pH values. Second, we investigated the effect of Fe dosage rate on arsenic removal in different pH and O_2 recharge scenarios. Finally, we assessed the robustness of the trends predicted by the model, which operates at constant pH, against lab experiments reproducing more realistic conditions where pH increases during treatment as a result of equilibration with atmospheric CO_2. Our results provide a nuanced understanding of the impact of operating conditions on arsenic removal by Fe-EC and can thus support the implementation of this technology at scale in a range of different groundwaters.

2. Methods

2.1. Arsenic removal experiments

A list of experiments conducted in this study, including detailed composition of each electrolyte, is given in Tables 1 and 2. The majority of experiments were conducted using

synthetic Bengal groundwater (SGW), which was prepared according to a procedure described elsewhere (Delaire et al., 2015). The composition of SGW (8.2 ± 0.1 mM HCO_3^-, 2.6 ± 0.2 mM Ca^{2+}, 1.9 ± 0.1 mM Mg^{2+}, 1.2 ± 0.1 mM Si, 0.12 ± 0.02 mM P, 10.9 ± 0.3 mM Na^+, 8.9 ± 0.5 mM Cl^-, and 494 ± 45 µg/L (6.6 ± 0.6 µM) As(III) ($NaAsO_2$ salt)) was similar to that of Roberts et al. (2004), which was derived from an extensive survey of arsenic-contaminated tubewells in Bangladesh by the British Geological Survey (2001). Fe-EC experiments were conducted by applying a galvanostatic current between two Fe(0) electrodes (each 98.0 ± 0.2 % Fe, 1.0 cm x 5.0 cm x 1 mm, 0.5 cm apart, submerged surface area of 1.5 cm^2) immersed in 195 mL SGW. Electrodes were cleaned with sand paper before each experiment to remove rust deposits. Operating conditions were selected based on previous studies to avoid the anodic production of chlorine or oxygen (Amrose et al., 2013; Li et al., 2012; van Genuchten et al., 2012). Current densities between 2.0 ± 0.4 and 20.0 ± 1.0 mA/cm^2 were applied, corresponding to Fe dosage rates of 0.9-9.3 ± 0.2 C/L/min according to Faraday's law. The electrolysis time was adjusted to achieve the desired Fe dosage (6-74 ± 1 mg/L). Electrolysis took place in open air and with solution mixing. After electrolysis (or the addition of $FeSO_4$ salts in some experiments, as indicated in Table 1), the solution was mixed in open air to achieve full Fe(II) oxidation (i.e. total Fe in the filtrate using 0.45 µm filter <0.1 mg/L). We verified in preliminary experiments that adsorption processes were faster than Fe(II) oxidation at circumneutral pH; therefore we defined the completion of Fe(II) oxidation as "equilibrium". Reaching equilibrium was necessary to conduct rigorous comparisons between operating conditions. Representative time profiles of As(III) and Fe(II) concentrations are presented in Figures S1 and S2. The pH was measured with a Consort pH meter (R3620). Two types of experiments were conducted (Tables 1 and 2): experiments in which the pH was held constant to calibrate the computational model (pH 6.6, 7.0, 7.5, and 8.1), and experiments in which the initial pH was allowed to drift to reproduce field operating conditions (initial pH of 6.0, 7.0, and 8.0; final pH as indicated). In constant-pH experiments, the solution pH was controlled by

adding drops of 1.1 M HCl as necessary (pH maintained within ± 0.2 pH units). In drift-pH experiments, the final pH ranged from 8.0 to 8.5 and was determined principally by equilibration with atmospheric CO_2 and not by initial pH. All experiments were replicated 2 to 5 times and the results were averaged. Unless specified otherwise (Figure 1), reported errors are the largest of the measurement error and the standard deviation of replicate experiments.

Measurements of As(III), total As, Fe, Si, P, Ca, and Mg were performed by inductively coupled plasma optical emission spectrometry (ICP-OES, PerkinElmer 5300 DV, measurement error typically < 5%). Unfiltered and filtered (0.45 μm nylon filters) 5 mL samples digested with 1 mL 1.1 M HCl were analyzed to determine total and dissolved concentrations of ions, respectively. Concentrations of adsorbed ions were calculated as the difference between total and dissolved concentrations. The concentration of Fe(II) was equated to the concentration of Fe in filtered samples because Fe(III) is insoluble at circumneutral pH. For As(III) measurements, digested samples were diluted 50 times in 0.25 M disodium citrate and analyzed with hydride generation, following Roberts et al. (2004) (measurement error typically <10%). As(V) was measured as the difference between total As and As(III).

2.2. Computational model

We adapted the computational model described in Li et al. (2012), which predicts the removal of As(III) and As(V) in the Fe-EC system assuming second-order kinetics for both Fe(II) oxidation by O_2 and As(III) oxidation by reactive species, and Langmuir adsorption isotherms for As(III), As(V), P, and Si. Accordingly, the equations governing this model are:

$$\frac{d[Fe(II)]}{dt} = D - k_{app}\,[Fe(II)]\,[O_2] \qquad (1)$$

$$\frac{d[As(III)]_{oxidized}}{dt} = \frac{\beta}{1 + \frac{k_1}{k_2}\frac{[Fe(II)]}{[As(III)]}}\,k_{app}\,[Fe(II)]\,[O_2] \qquad (2)$$

$$[As(III), As(V), P, Si]_{adsorbed} = \frac{q_{max}\,[Fe(III)]\,K_{As(III),As(V),P,Si}\,[As(III), As(V), P, Si]}{1 + K_{As(III)}[As(III)] + K_{As(V)}[As(V)] + K_{Si}[Si] + K_P[P]} \quad (3)$$

where D (M s^{-1}) is the Fe dosage rate; k_{app} (M^{-1} s^{-1}) is the second order rate constant for Fe(II) oxidation by O_2; β is the yield of reactive intermediates (Fe(IV)) from Fe(II) oxidation by O_2 and was determined to be ~ 0.25 by Li et al. (2012); $\frac{k_1}{k_2}$ is the relative affinity of reactive intermediates for Fe(II) compared to As(III); q_{max} (dimensionless) is the adsorption capacity of EC precipitates generated in SGW; and $K_{As(III),As(V),P,Si}$ (M^{-1}) are the adsorption affinities of EC precipitates for As(III), As(V), Si, and P, respectively. Previous work has shown that the model accurately predicts the time-dependent concentration of Fe(II) (Li et al., 2012). We added a fourth equation to describe the time-dependent concentration of O_2, in which $[O_2]_{saturation}$ is equal to 0.25 mM at 25 ºC and k_r (s^{-1}) is the O_2 recharge rate resulting from mixing and aeration:

$$\frac{d[O_2]}{dt} = k_r * ([O_2]_{saturation} - [O_2]) - k_{app} * [Fe(II)] * [O_2] \quad (4)$$

K_{Si} and $K_{As(III)}$ are not expected to vary significantly between pH 6.6 and 8.1 (Dixit and Hering, 2003) because Si and As(III) do not deprotonate in this pH range (first pK_As of H_4SiO_4 and H_3AsO_3 are > 9) (Benjamin, 2000). Therefore, we used values measured by Li et al. (2012), K_{Si}=$10^{2.94}$ and $K_{As(III)}$=$10^{3.81}$, which were comparable to values reported in other studies for similar systems (Li et al., 2014; Roberts et al., 2004). In contrast, k_{app}, $\frac{k_1}{k_2}$, $K_{As(V)}$, K_P, and q_{max} may all be pH-dependent. The computational model was implemented in Python 2.7 (Python Software Foundation) and the solver was the *fsolve* method in *scipy.optimize* (Jones et al., 2001).

2.3. Determining adsorption and oxidation rate constants at different pH values

To determine $K_{As(V)}$, K_P, and q_{max} within our electrolyte across different pH values, Fe-EC experiments were conducted at a Fe dosage rate of 9.2 ± 0.2 C/L/min and at a Fe dosage of 29 ± 1 mg/L in SGW amended with high concentrations of As and P (relative to values commonly measured in arsenic contaminated aquifers in Bengal) for improved sensitivity (column 1 in Tables 1 and 2). Dissolved and adsorbed concentrations of Si, P, As(III), and As(V) were measured at equilibrium (i.e. after full Fe(II) oxidation, as defined above, which required 60 to 240 min of post-electrolysis mixing depending on pH) and computed in Equations 5-7, which derive from Equation 3 (see SI):

$$K_{As(V)} = K_{Si}\,\frac{[Si]}{[As(V)]}\,\frac{[As(V)]_{adsorbed}}{[Si]_{adsorbed}} \qquad (5)$$

$$K_P = K_{Si}\,\frac{[Si]}{[P]}\,\frac{[P]_{adsorbed}}{[Si]_{adsorbed}} \qquad (6)$$

$$q_{max} = \frac{[Si]_{adsorbed}}{K_{Si}\,[Si]}\,\frac{1 + K_{As(III)}[As(III)] + K_{As(V)}[As(V)] + K_{Si}[Si] + K_P[P]}{[Fe(III)]} \qquad (7)$$

To determine k_{app} and $\frac{k_1}{k_2}$ within our electrolyte across different pH values, 31 ± 1 mg/L $FeSO_4$ was added to SGW amended with a high concentration of As(III) (for improved sensitivity) and mixed in open air for 6 to 60 minutes depending on pH (column 2 in Tables 1 and 2). Fe(II) and total As(III) (total As(III) = adsorbed As(III) + dissolved As(III)), were measured at regular time intervals (Figure S2). k_{app} at a given pH was determined by fitting the concentration of Fe(II) as a function of time to Equation 8, which derives from Equation 1 (D=0 C/L/min after $FeSO_4$ addition). The concentration of O_2 was assumed to be saturated (0.25 mM) following Li et al. (2012).

$$[Fe(II)](t) = [Fe(II)]_{t=0}\,e^{-k_{app}\,[O_2]\,t} \qquad (8)$$

Although it also appears in the equation governing As(III) (Equation 2), k_{app} was determined by solely fitting the concentration of Fe(II) (Equation 8) because it is intrinsically linked to

Fe(II), and not to As(III). Using the determined value of k_{app}, $\frac{k_1}{k_2}$ for the same pH was determined by fitting the concentration of As(III) over time to Equation 2. An example of this procedure at pH 7.0 is shown in Figure S2. Average R^2 goodness-of-fit values for Fe(II) and As(III) concentrations over time were 0.95 and 0.89, respectively (R^2 values for each pH are provided in Table S1).

The means and 95% confidence intervals of adsorption and oxidation rate constants measured in duplicate at pH 6.6, 7.0, 7.5, and 8.1 are presented in Figure 1a-b (summarized in Table S2). We conducted model simulations using "mean" constants and compared them against a third set of experiments, designed to be representative of field operations (in terms of As/P concentrations and Fe dosage rate, see column 3 in Tables 1 and 2). Because we observed non-negligible discrepancies between modeled and experimental arsenic concentrations (Figure S3), we adjusted the constants to achieve a better fit. To do that, we first evaluated the sensitivity of modeled arsenic removal to each individual constant, at each pH value. Using this sensitivity analysis, we then adjusted each constant within the range of duplicate measurements to minimize the discrepancy between modeled and experimental arsenic removal. Adjusted ("best-fit") adsorption and oxidation rate constants are indicated in red in Figure 1a-b and Table S2. The resulting "best fit" between modeled and experimental arsenic concentrations is shown in Figure 2 (compare with the poorer fit in Figure S3). Model simulations conducted in the rest of the paper use "best-fit" adsorption and oxidation rate constants (as opposed to "mean" constants).

2.4. Model simulations

The model was operated with initial As(III), As(V), Si, and P concentrations of 500 µg/L, 0 µg/L, 34.2 mg/L, and 3.7 mg/L, respectively. To investigate the effect of pH on the mechanisms of arsenic removal, simulations were conducted at pH 6.6, 7.0, 7.5, and 8.1 for a range of Fe dosages (5 to 50 mg/L in 3 mg/L increments), using a Fe dosage rate of 3 C/L/min.

Analyzing the respective concentrations of dissolved and adsorbed As(III)/As(V) allowed us to identify the processes limiting arsenic removal at each pH. Then, we sequentially investigated the effect of operating conditions on arsenic removal at each pH (using a fixed total Fe dosage of 30 mg/L); progressively adding in complexity, we first conducted simulations at varying Fe dosage rates (0.5 to 20 C/L/min) and at O_2 saturation, and then at both varying Fe dosage rates (0.5 to 80 C/L/min) and O_2 recharge rates (2.0 hr^{-1}, 4.6 hr^{-1}, and at O_2 saturation). O_2 recharge rates of 2.0 and 4.6 hr^{-1} were chosen to represent the mixing regimes of a 200 mL beaker with an area-to-volume ratio of 0.3 (assuming an air-water exchange coefficient of $1.9x10^{-3}$ cm/s, consistent with Rantakari et al. (2015)), and an actively aerated reactor in a wastewater treatment plant (Hunt, 2013), respectively. Unless indicated otherwise, simulations included a post-electrolysis mixing period (i.e. with D=0 in Equation 1) long enough to achieve 99.99% Fe(II) oxidation, which we defined as "equilibrium". When equilibrium required over 100 min of post-electrolysis mixing, which is a realistic upper bound for field operations, we reported arsenic removal both at equilibrium and after 100 min of mixing.

2.5. Comparison between model simulations and experiments representative of field conditions

A series of experiments was conducted in SGW without holding pH constant to reproduce realistic field conditions where pH evolves due to equilibration with atmospheric CO_2. These experiments were performed for five different dosages (6.5 ± 1.1, 13.1 ± 2.4, 24.5 ± 5.8, 48.4 ± 6.1, and 68.9 ± 6.8 mg/L) at three Fe dosage rates (0.9, 3.1, and 9.3 ± 0.2 C/L/min) and three initial pH values (6.0, 7.0, and 8.0, see Table 1). Model predictions regarding the effect of pH and Fe dosage rate were compared to drift-pH experiments to assess their generalizability in realistic field conditions. In these simulations, the model was operated at O_2 saturation, which is a reasonable assumption for a 200 mL beaker vigorously stirred in open air.

3. Results and Discussion

3.1. Adsorption and oxidation rate constants

Experimentally determined adsorption constants K_P, $K_{As(V)}$, and q_{max}, are presented in Figure 1a and Table S2. Higher adsorption affinities for P than for As(V) are consistent with previous studies in similar systems (Li et al., 2014; Roberts et al., 2004; van Genuchten et al., 2014a). We found that the affinity of EC precipitates for P and As(V) decreases by 0.65 and 0.53 log, respectively, for each unit increase in pH. This finding is consistent with previous studies, which report lower As(V)/P adsorption to Fe(III) (oxyhydr)oxides with increasing pH (Dixit and Hering, 2003; Gao and Mucci, 2001) due to a higher electrostatic barrier to anions when surface groups deprotonate. Values of $K_{As(V)}$ determined in this study were generally consistent with existing data on As(V) adsorption to hydrous ferric oxides (Dixit and Hering, 2003) (see a comparison in Figure S4). Interestingly, the adsorption capacity of EC precipitates, q_{max}, was found to slightly increase with pH. ICP-OES measurements also indicated substantial increases in Ca and Mg uptake between pH 6.6 and 8.1 (by ~200% on average, Table S3). Previous work has shown that the uptake of bivalent cations by Fe(III) precipitates, which occurs both electrostatically and via ternary surface complexes (e.g. Ca-P-Fe or Ca-As(V)-Fe), enhances the removal of oxyanions (van Genuchten et al., 2014a). Presumably, such improvement in oxyanion uptake is partly due to increased precipitate capacity in the presence of bound bivalent cations, which may provide additional adsorption sites or increase the accessibility of existing ones (by decreasing the electrostatic barrier). Therefore, we propose that the observed increase in q_{max} with pH results from enhanced bivalent cation uptake, which may be favored at higher pH due to P/As(V) deprotonation ($pK_{a,2}$ = 7.2 and 6.9, respectively).

Experimentally determined oxidation rate constants are shown in Figure 1b and Table S2. We

found that the oxidation rate of Fe(II) by O_2 in SGW, k_{app}, increases by 1.6 orders of magnitude for each unit increase in pH, which is comparable to the pH-dependency measured in other carbonated systems in the same pH range (~1.7) (Emmenegger et al., 1998; King, 1998). We also found that $\frac{k_1}{k_2}$ increases approximately threefold between pH 6.6 and 8.1, which indicates a decrease in the relative affinity of reactive intermediates for As(III) compared to Fe(II). Although As(III) and Fe(II) both become easier to oxidize at higher pH due to increased concentrations of deprotonated and carbonated species, respectively (King, 1998; Pettine et al., 1999), our results suggest that this effect is slightly stronger for Fe(II) in SGW. This is consistent with the stronger pH dependence of the oxidation potential of Fe(II) compared to that of As(III) at circumneutral pH (see Pourbaix diagrams in Ruby et al. (2010) and Smedley and Kinniburgh (2002), respectively).

Modeled and experimental post-treatment arsenic concentrations are presented in Figure 2, showing good agreement in the majority of cases. However, our model overestimates removal for low Fe dosages (< 25 mg/L) at pH 7.0 and 7.5, and underestimates it for high dosages (>35 mg/L) at pH 8.1. Adsorption and oxidation rate constants, which are assumed to be independent of the Fe concentration in our model, were measured at a Fe dosage of 30 ± 2 mg/L (Table 1). The observed discrepancies between the model and experiments at Fe dosages significantly different from 30 mg/L suggest that model constants may actually depend on the Fe dosage. For example, Langmuir isotherms may not be able to precisely model adsorption processes in systems such as Fe-EC, where the structure and reactivity of the adsorbent strongly depend on the molar ratio of Fe : oxyanions : bivalent cations (van Genuchten et al., 2014a, 2014b).

3.2. Effect of pH on arsenic removal with Fe-EC

Figure 3a shows post-treatment arsenic concentrations as a function of Fe dosage according to model simulations at different pH values (using a fixed Fe dosage rate of 3 C/L/min). Except at pH 6.6, 99.99% Fe(II) oxidation is achieved with post-electrolysis mixing times below 100 min (1, 10, and 100 min at pH 8.1, 7.5, and 7.0, respectively). At pH 6.6, approximately 99% of Fe(II) is oxidized after 100 min mixing, whereas full (>99.99%) oxidation requires 300 min. When mixing time is constrained to be ≤ 100 min, the post-treatment dissolved arsenic concentration for a given Fe dosage decreases with increasing pH (Figure 3a), despite decreased precipitate affinity for As(V) (i.e. decreasing $K_{As(V)}$) and decreased As(III) competitiveness for reactive intermediates (i.e. increasing $\frac{k_1}{k_2}$). Thus, our results show that the impact of a higher pH on arsenic removal is dominated by the beneficial effect of faster Fe(II) oxidation kinetics, which limit the accumulation of Fe(II) and thus the scavenging of reactive intermediates needed to oxidize As(III) to As(V). Simulations at pH 6.6 show that the extent of arsenic removal is significantly enhanced (removing an additional 20 to 60 µg/L arsenic depending on the Fe dosage) when the mixing time is extended from 100 to 300 min to improve Fe(II) oxidation from 99% to 99.99%, due to improved As(III) oxidation. During the late stages of mixing, competition for reactive intermediates is minimized because Fe(II) is present in only trace concentrations, resulting in significant As(III) oxidation. This result illustrates that substantial improvements in arsenic removal can be achieved by increasing the post-electrolysis mixing time to oxidize trace levels of Fe(II), with the corresponding trade-off of increasing the total treatment time.

Figure 4 shows the speciation of arsenic in the same simulations as Figure 3a. At all pH values and all dosages, adsorbed As(III) is much smaller than adsorbed As(V), indicating that As(V) adsorption is either the primary (pH 6.6, 7.0, and 7.5) or the only (pH 8.1) mechanism of arsenic removal. At pH 6.6 and 7.0, As(III) accounts for the vast majority of dissolved arsenic, and As(III) adsorption does not increase for Fe dosages above 30 mg/L, indicating that arsenic

removal is limited primarily by the oxidation of As(III) to As(V). In contrast, at pH 8.1, As(V) accounts for the entirety of dissolved arsenic, indicating that removal is limited by As(V) adsorption. pH 7.5 represents an intermediary situation: at low Fe dosages (<35 mg/L), dissolved arsenic is composed of both As(III) and As(V) and arsenic removal is limited by both As(III) oxidation and As(V) adsorption. However, at higher dosages (>35 mg/L), As(V) accounts for the entirety of dissolved arsenic and removal is therefore limited by As(V) adsorption, similar to pH 8.1.

As pH increases, the process limiting arsenic removal thus shifts from As(III) oxidation to As(V) adsorption. This shift can be interpreted as follows. At lower pH values (6.6 and 7.0), the affinity of EC precipitates for As(V) ($K_{As(V)}$) is the highest and As(V) is adsorbed as soon as it forms, as supported by negligible concentrations of dissolved As(V) for Fe dosages > 20 mg/L in Figures 4a and 4b. However, slow Fe(II) oxidation kinetics lead to the accumulation of Fe(II), which competes with As(III) for reactive intermediates, leaving a large fraction of arsenic unoxidized and dissolved. In contrast, faster Fe(II) oxidation kinetics at higher pH values (7.5 and 8.1) favor the oxidation of As(III), which disappears for Fe dosages >30 mg/L at pH 7.5 and >10 mg/L at pH 8.1 (Figures 4c and 4d). At these higher pH values, decreased precipitate affinity for As(V) limits adsorption, explaining the higher concentrations of dissolved As(V) compared to lower pH values.

We note that the small model inaccuracies (Figure 2) should not affect our mechanistic analysis, which relies on general trends in arsenic speciation over a large range of Fe dosages (Figure 4) encompassing the range in which the model is most accurate. In the following section, the model was operated at 30 mg/L, the Fe dosage at which model constants were measured.

3.3. Impact of Fe dosage rate on arsenic removal at different pH values

Figure 3b shows post-treatment arsenic concentrations as a function of Fe dosage rate in model simulations at different pH values, using a constant Fe dosage of 30 mg/L. The impact of the Fe dosage rate on arsenic removal strongly depends on pH. At lower pH values (6.6 and 7.0), increasing the Fe dosage rate from 0.5 to 5 C/L/min strongly inhibits arsenic removal, while further increases in Fe dosage rate have a minimal impact. At pH 7.5, increases in Fe dosage rate between 2 and 20 C/L/min lead to a more gradual decrease in arsenic removal. In contrast, at pH 8.1, arsenic removal is independent of the Fe dosage rate between 0.5 and 20 C/L/min.

The Fe dosage rate affects the accumulation of Fe(II) and thus the kinetics of As(III) oxidation (Equation 2) (Li et al., 2012). Consequently, the Fe dosage rate is expected to have a strong impact when arsenic removal is primarily limited by As(III) oxidation (e.g. at 3 C/L/min for pH 6.6 and 7.0, Figures 4a and 4b), and a smaller impact when arsenic removal is primarily limited by As(V) adsorption (e.g. at 3 C/L/min for pH 7.5 and 8.1, Figures 4c and 4d), which is consistent with the model predictions in Figure 3b. At pH 7.5, the increasing sensitivity of arsenic removal to Fe dosage rate between 0.5 and 10 C/L/min reflects a shift in the process that primarily limits arsenic removal from As(V) adsorption to As(III) oxidation (Figure S5a-b).

For pH 6.6, 7.0, and 7.5, the effect of the Fe dosage rate on arsenic removal in Figure 3b levels off at high dosage rates, indicating that arsenic removal becomes independent of the Fe dosage rate. However, we note that this behavior does not reflect a change in the process limiting arsenic removal, which remains As(III) oxidation (Figure S5c). At high Fe dosage rates, where the concentration of Fe(II) is large, Equation 2 can be simplified into Equation 9. The kinetics of As(III) oxidation are therefore no longer controlled by the concentration of Fe(II) and are independent of the Fe dosage rate.

$$\frac{d[As(III)]_{oxidized}}{dt} = \beta \frac{k_2}{k_1} k_{app} [O_2] [As(III)] \quad (9)$$

3.4. Impact of O_2 recharge rate on arsenic removal at different pH values and Fe dosage rates

Figure 5 shows the effect of Fe dosage rate on arsenic removal for several O_2 recharge rates. Overall, the model predicts lower arsenic removal when O_2 consumption by Fe(II) oxidation is taken into account. O_2 recharge rates of 2.0 and 4.6 hr^{-1} are not sufficient to prevent significant O_2 depletion during treatment. For example, at pH 7.0 and 3 C/L/min, O_2 levels decrease to 28% and 49% of saturation for recharge rates of 2.0 and 4.6 hr^{-1}, respectively, with the effect of O_2 depletion on arsenic removal becoming more pronounced at higher pH values and larger Fe dosage rates. Lower O_2 concentrations promote Fe(II) accumulation, which inhibits As(III) oxidation and reduces arsenic removal. Figure 5 shows that O_2 depletion exacerbates the sensitivity of arsenic removal to Fe dosage rate, indicating that arsenic removal is predominantly limited by As(III) oxidation when O_2 saturation is not maintained.

3.5. Comparison between model simulations and experiments representative of field conditions

Figure 6a shows post-treatment arsenic concentrations and pH values as a function of Fe dosage in pH-drift experiments with initial pH values of 6.0, 7.0, and 8.0. Results from model simulations are shown to depict the expected effect of pH when it is held constant. pH-drift experiments exhibited a trend of improved arsenic removal at higher initial pH, but this trend was substantially less pronounced than in model predictions: because the pH drifted to ~8.0-8.5 independent of its initial value, the effect of pH on arsenic removal was partly cancelled.

Figure 6b presents post-treatment arsenic concentrations as a function of Fe dosage for drift-pH experiments conducted at an initial pH of 7.0 and at two Fe dosage rates (0.9 and 9.3 ± 0.2 C/L/min). Arsenic concentrations after both 20 and 120 min post-electrolysis mixing are reported, as well as corresponding solution pH values. Results from model simulations are shown to depict the effect of Fe dosage rate expected at constant pH. In pH-drift experiments, pH invariably increased from 7.0 to 8.0-8.5. Therefore, arsenic removal could have been expected to be less limited by As(III) oxidation (Figure 4) and less sensitive to Fe dosage rate (Figure 3b) compared to constant-pH experiments. In contrast, lowering the Fe dosage rate in pH-drift experiments improved arsenic removal more than predicted by the constant-pH model. As shown in Figure 6b, arsenic concentrations did not vary significantly after 20 min of post-electrolysis mixing, indicating that most of the arsenic was removed before the end of the shorter mixing period. Therefore, in experiments at 9.3 C/L/min, arsenic removal took place at pH <7.7-8.1 (Figure 6b). In contrast, in experiments at 0.9 C/L/min, which had tenfold longer dosage times, pH increased up to 8.2-8.6 before the majority of arsenic removal was achieved. Consequently, arsenic removal at 0.9 C/L/min overall took place at substantially higher pH values than in experiments at 9.3 C/L/min, likely contributing to the improved performance at lower Fe dosage rates. We propose that in field-like conditions in which pH increases over time (as carbonate-rich groundwater equilibrates with atmospheric CO_2), improved Fe-EC performance at lower Fe dosage rates is partly explained by the deferment of reactions until pH has significantly increased, which favors arsenic removal (Figure 3a).

4. Conclusions

Our results show that pH controls the impact that operating conditions can have on arsenic removal in Fe-EC. While a previous study (at pH 7.1) had found that decreasing the Fe dosage rate could improve the performance of Fe-EC (Li et al., 2012), we demonstrated that this finding only applies when arsenic removal is limited by As(III) oxidation, i.e. at low pH (<

7.5). In contrast, decreasing the Fe dosage rate at pH>8.0 would only extend the duration of treatment without any benefits to arsenic removal. However, we also found that if oxygen saturation cannot be maintained, decreasing the Fe dosage rate is preferable at any pH. Finally, our results show that increasing the O_2 recharge rate without achieving O_2 saturation can have little to no effect on arsenic removal, especially at higher pH values.

We found that the trends predicted by our constant-pH model, such as improved arsenic removal at higher pH and at lower Fe dosage rate, are still valid – though not of the same magnitude– in more realistic experiments in which pH is not held constant. This result indicates that our model can serve as a useful tool to inform decisions about the operation of Fe-EC in the field. We note that the pH drift in our lab experiments may be larger than during typical field treatment (pH increased < 0.5 in a field trial of Fe-EC in West Bengal, India (Amrose et al., 2014)), possibly due to better air-water exchange in the lab setup. The actual effect of initial pH in the field may therefore be larger than reported in Figure 6a, while the actual effect of Fe dosage rate may be smaller than reported in Figure 6b.

Finally, our model can still be improved. Although it already accounts for a number of groundwater characteristics (pH, concentrations of oxyanions) and operating conditions (Fe dosage rate, post-electrolysis mixing time, O_2 recharge rate), more work is needed to incorporate the beneficial effect of bivalent cations on the uptake of oxyanions by Fe(III) (oxyhydr)oxide precipitates (van Genuchten et al., 2014a; Voegelin et al., 2010) as well as CO_2 dynamics. Measuring the O_2 recharge rate in field conditions is also needed. In addition, future efforts to further improve the model could investigate equations different from the Langmuir isotherm that may better describe adsorption in Fe-EC, where the adsorbent is generated in the presence of adsorbates and bivalent cations.

Acknowledgements

The authors want to express their gratitude to Nathan Addy and Akshay Shrivastava for developing the model in Python. This work was supported by the Development Impact Lab (USAID Cooperative Agreement AID-OAA-A-13-00002), part of the USAID Higher Education Solutions Network; by the Andrew and Virginia Rudd Family Foundation Chair for Safe Water and Sanitation administered by the Blum Center for Developing Economies; and by a fellowship to M. Z. from the Civil and Environmental Engineering Department at UC Berkeley.

References

Amrose, S., Gadgil, A., Srinivasan, V., Kowolik, K., Muller, M., Huang, J., Kostecki, R., 2013. Arsenic removal from groundwater using iron electrocoagulation: effect of charge dosage rate. J. Environ. Sci. Health. A. Tox. Hazard. Subst. Environ. Eng. 48, 1019–30. doi:10.1080/10934529.2013.773215

Amrose, S.E., Bandaru, S.R.S., Delaire, C., van Genuchten, C.M., Dutta, A., DebSarkar, A., Orr, C., Roy, J., Das, A., Gadgil, A.J., 2014. Electro-chemical arsenic remediation: field trials in West Bengal. Sci. Total Environ. 488–489, 539–46. doi:10.1016/j.scitotenv.2013.11.074

Benjamin, M.M., 2000. Water Chemistry, 3rd ed.

British Geological Survey, 2001. Arsenic contamination of groundwater in Bangladesh [WWW Document]. URL http://www.bgs.ac.uk/research/groundwater/health/arsenic/Bangladesh/data.html (accessed 5.22.15).

Chakraborti, D., Rahman, M.M., Das, B., Nayak, B., Pal, A., Sengupta, M.K., Hossain, M.A., Ahamed, S., Sahu, M., Saha, K.C., Mukherjee, S.C., Pati, S., Dutta, R.N., Quamruzzaman, Q., 2013. Groundwater arsenic contamination in Ganga–Meghna–Brahmaputra plain, its health effects and an approach for mitigation. Environ. Earth Sci. 70, 1993–2008. doi:10.1007/s12665-013-2699-y

Delaire, C., van Genuchten, C.M., Nelson, K.L., Amrose, S.E., Gadgil, A.J., 2015. Escherichia coli Attenuation by Fe Electrocoagulation in Synthetic Bengal Groundwater: Effect of pH and Natural Organic Matter. Environ. Sci. Technol. 49, 9945–53. doi:10.1021/acs.est.5b01696

Dixit, S., Hering, J.G., 2003. Comparison of Arsenic(V) and Arsenic(III) Sorption onto Iron Oxide Minerals: Implications for Arsenic Mobility. Environ. Sci. Technol. 37, 4182–4189. doi:10.1021/es030309t

Emmenegger, L., King, D.W., Sigg, L., Sulzberger, B., 1998. Oxidation Kinetics of Fe(II) in a Eutrophic Swiss Lake. Environ. Sci. Technol. 32, 2990–2996. doi:10.1021/es980207g

Gao, Y., Mucci, A., 2001. Acid base reactions, phosphate and arsenate complexation, and their competitive adsorption at the surface of goethite in 0.7 M NaCl solution. Geochim. Cosmochim. Acta 65, 2361–2378. doi:10.1016/S0016-7037(01)00589-0

Holt, P.K., Barton, G.W., Mitchell, C.A., 2005. The future for electrocoagulation as a localised water treatment technology. Chemosphere 59, 355–67. doi:10.1016/j.chemosphere.2004.10.023

Hug, S.J., Leupin, O., 2003. Iron-catalyzed oxidation of arsenic(III) by oxygen and by hydrogen peroxide: pH-dependent formation of oxidants in the Fenton reaction. Environ. Sci. Technol. 37, 2734–42.

Hunt, J.R., 2013. Reader for CE 211A, Environmental Physical-Chemical Processes for Water Treatment, UC Berkeley.

Jones, E., Oliphant, T., Peterson, P., and others, 2001. SciPy: Open Source Scientific Tools for

Python.

King, D.W., 1998. Role of Carbonate Speciation on the Oxidation Rate of Fe(II) in Aquatic Systems. Environ. Sci. Technol. 32, 2997–3003. doi:10.1021/es980206o

Li, L., Li, J., Shao, C., Zhang, K., Yu, S., Gao, N., Deng, Y., Yin, D., 2014. Arsenic removal in synthetic ground water using iron electrolysis. Sep. Purif. Technol. 122, 225–230. doi:10.1016/j.seppur.2013.11.012

Li, L., van Genuchten, C.M., Addy, S.E.A., Yao, J., Gao, N., Gadgil, A.J., 2012. Modeling As(III) oxidation and removal with iron electrocoagulation in groundwater. Environ. Sci. Technol. 46, 12038–45. doi:10.1021/es302456b

Neumann, A., Kaegi, R., Voegelin, A., Hussam, A., Munir, A.K.M., Hug, S.J., 2013. Arsenic removal with composite iron matrix filters in Bangladesh: a field and laboratory study. Environ. Sci. Technol. 47, 4544–54. doi:10.1021/es305176x

Pettine, M., Campanella, L., Millero, F.J., 1999. Arsenite oxidation by H2O2 in aqueous solutions. Geochim. Cosmochim. Acta 63, 2727–2735. doi:10.1016/S0016-7037(99)00212-4

Python Software Foundation, n.d. Python Language Reference, version 2.7.

Rantakari, M., Heiskanen, J., Mammarella, I., Tulonen, T., Linnaluoma, J., Kankaala, P., Ojala, A., 2015. Different Apparent Gas Exchange Coefficients for CO2 and CH4: Comparing a Brown-Water and a Clear-Water Lake in the Boreal Zone during the Whole Growing Season. Environ. Sci. Technol. 49, 11388–94. doi:10.1021/acs.est.5b01261

Ravenscroft, P., Brammer, H., Richards, K., 2009. Arsenic Pollution: A Global Synthesis. Wiley-Blackwell, Oxford, UK. doi:10.1002/9781444308785

Roberts, L.C., Hug, S.J., Ruettimann, T., Billah, M.M., Khan, A.W., Rahman, M.T., 2004. Arsenic Removal with Iron(II) and Iron(III) in Waters with High Silicate and Phosphate Concentrations. Environ. Sci. Technol. 38, 307–315. doi:10.1021/es0343205

Ruby, C., Abdelmoula, M., Naille, S., Renard, A., Khare, V., Ona-Nguema, G., Morin, G., Génin, J.-M.R., 2010. Oxidation modes and thermodynamics of FeII–III oxyhydroxycarbonate green rust: Dissolution–precipitation versus in situ deprotonation. Geochim. Cosmochim. Acta 74, 953–966. doi:10.1016/j.gca.2009.10.030

Smedley, P.., Kinniburgh, D.., 2002. A review of the source, behaviour and distribution of arsenic in natural waters. Appl. Geochemistry 17, 517–568. doi:10.1016/S0883-2927(02)00018-5

van Genuchten, C.M., Addy, S.E.A., Peña, J., Gadgil, A.J., 2012. Removing arsenic from synthetic groundwater with iron electrocoagulation: an Fe and As K-edge EXAFS study. Environ. Sci. Technol. 46, 986–94. doi:10.1021/es201913a

van Genuchten, C.M., Gadgil, A.J., Peña, J., 2014a. Fe(III) nucleation in the presence of bivalent cations and oxyanions leads to subnanoscale 7 Å polymers. Environ. Sci. Technol. 48, 11828–36. doi:10.1021/es503281a

van Genuchten, C.M., Peña, J., Amrose, S.E., Gadgil, A.J., 2014b. Structure of Fe(III) precipitates generated by the electrolytic dissolution of Fe(0) in the presence of

517 groundwater ions. Geochim. Cosmochim. Acta 127, 285–304.
518 doi:10.1016/j.gca.2013.11.044

519 Voegelin, A., Kaegi, R., Frommer, J., Vantelon, D., Hug, S.J., 2010. Effect of phosphate,
520 silicate, and Ca on Fe(III)-precipitates formed in aerated Fe(II)- and As(III)-containing
521 water studied by X-ray absorption spectroscopy. Geochim. Cosmochim. Acta 74, 164–
522 186. doi:10.1016/j.gca.2009.09.020

523

Tables and Figures

Table 1: Detailed operating conditions for all experiments conducted in this study. [a] SGW= synthetic Bengal groundwater; specific composition detailed in Table 2. [b] Uncertainty of Fe dosage rate is ± 0.2 C/L/min. [c] Initial pH; pH was then allowed to drift during the experiment.

	***MODEL CALIBRATIONS* (Constant pH)**												***REALISTIC SCENARIO***		
	1				**2**				**3**				**4**		
	Measurement of adsorption constants				**Measurement of oxidation rate constants**				**Model optimization**				**pH drift experiments**		
Electrolyte	SGW[a] with high As/P				SGW[a] with high As				SGW[a]				SGW[a]		
Fe dosage type	Fe-EC				$FeSO_4$				Fe-EC				Fe-EC		
pH	6.6	7.0	7.5	8.1	6.6	7.0	7.5	8.1	6.6	7.0	7.5	8.1	6.0[c]	7.0[c]	8.0[c]
Fe dosage rate (C/L/min)[b]	9.2				N/A				2.2				3.1	0.9 3.1 9.3	3.1
Total Fe dosage (mg/L)	29 (±1)				31 (±1)				19-41 (±3)				6-74 (±1)		
Post-electrolysis equilibration time (min)	240	90	60	60	60	60	20	6	240	90	60	60	120		

Table 2: Detailed electrolyte composition for all experiments conducted in this study. Concentrations of As(III), Ca^{2+}, Mg^{2+}, Si, and P were measured with ICP-OES. The target concentration of HCO_3^- was 8.2 mM but it was not directly measured. Concentrations of Na^+ and Cl^- were calculated from the concentrations of Si/P/HCO_3^- and Ca^{2+}/Mg^{2+}, respectively, because they were added as a salt with these ions. We present averages and standard deviations from replicate experiments. Major differences from synthetic Bengal groundwater (SGW) are highlighted in red. *For the measurement of adsorption constants (column 1), As(V) was used instead of As(III) in one replicate for simplicity, as the initial As speciation was not expected to affect the affinity of EC precipitates for As(V) or P.

	***MODEL CALIBRATIONS* (Constant pH)**						***REALISTIC SCENARIO***	
	1		**2**		**3**		**4**	
	Measurement of adsorption constants		**Measurement of oxidation rate constants**		**Model optimization**		**pH drift experiments**	
	Avg.	*St. dev.*	Avg.	*St. dev.*	Avg.	*St. dev.*	Avg.	*St. dev.*
As(III)* (µg/L) (and in µM)	2031 (27.1)	*75 (1.0)*	1972 (26.3)	*37 (0.5)*	522 (7.0)	*14 (0.2)*	470 (6.3)	*42 (0.6)*
Ca^{2+} (mM)	2.6	*0.2*	2.5	*0.1*	2.6	*0.1*	2.6	*0.1*
Mg^{2+} (mM)	1.8	*0.1*	1.8	*0.0*	2.0	*0.1*	1.9	*0.1*
Si (mM)	1.2	*0.1*	1.2	*0.0*	1.2	*0.1*	1.3	*0.1*
P (mM)	0.6	*0.0*	0.1	*0.0*	0.1	*0.0*	0.1	*0.0*
HCO_3^- (mM)	8.2	*0.1*	8.2	*0.1*	8.2	*0.1*	8.2	*0.1*
Na^+ (mM)	11.9	*0.3*	10.9	*0.2*	10.9	*0.2*	10.9	*0.3*
Cl^- (mM)	8.8	*0.5*	8.6	*0.2*	9.2	*0.4*	9.0	*0.5*

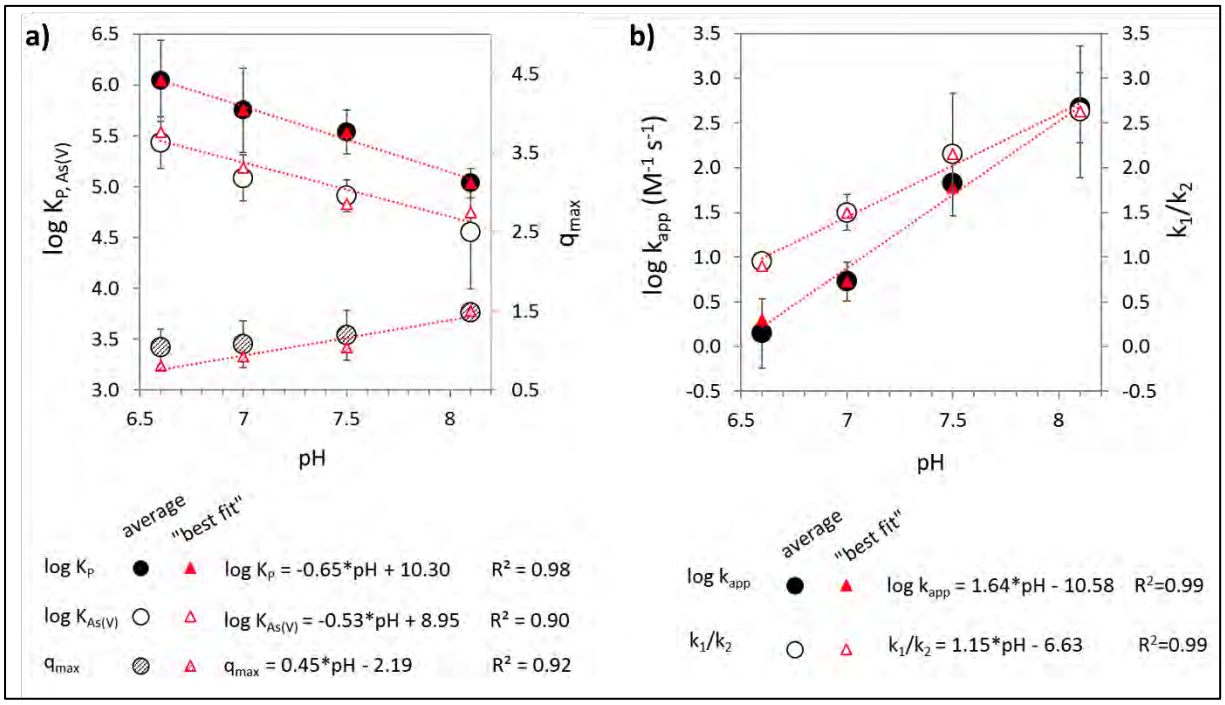

Figure 1: Adsorption (panel a) and oxidation rate (panel b) constants measured at pH 6.6, 7.0, 7.5, and 8.1. Averages and 95% confidence intervals from duplicate experiments are indicated (black and white circles), as well as the constants chosen in the final model ("best fit," red triangles).

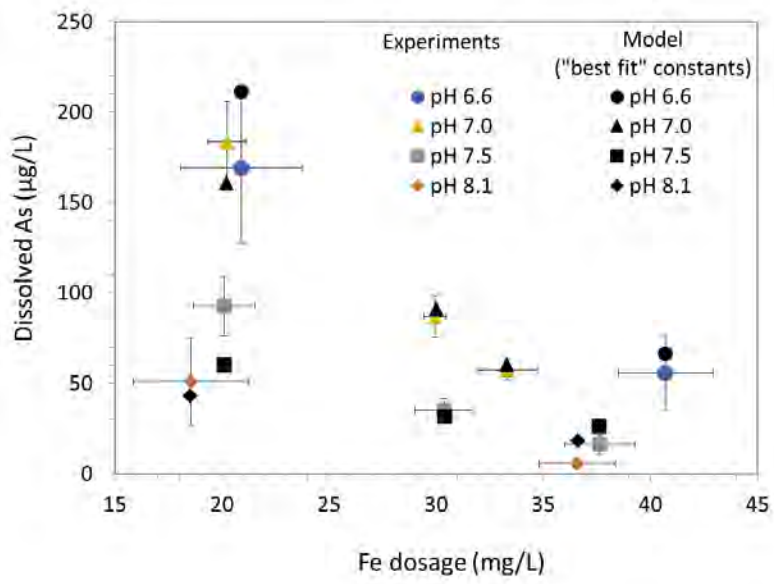

Figure 2: Comparison between experimental (colored shapes) and modeled (using "best fit" constants, black shapes) post-treatment arsenic concentrations at pH 6.6, 7.0, 7.5, and 8.1, using an initial As(III) concentration of 522 ± 14 µg/L, a Fe dosage rate of 2.2 C/L/min, and post-electrolysis mixing times between 60 and 240 min depending on pH (Table 1). Error bars are the largest of the measurement error and the standard deviation of replicate experiments.

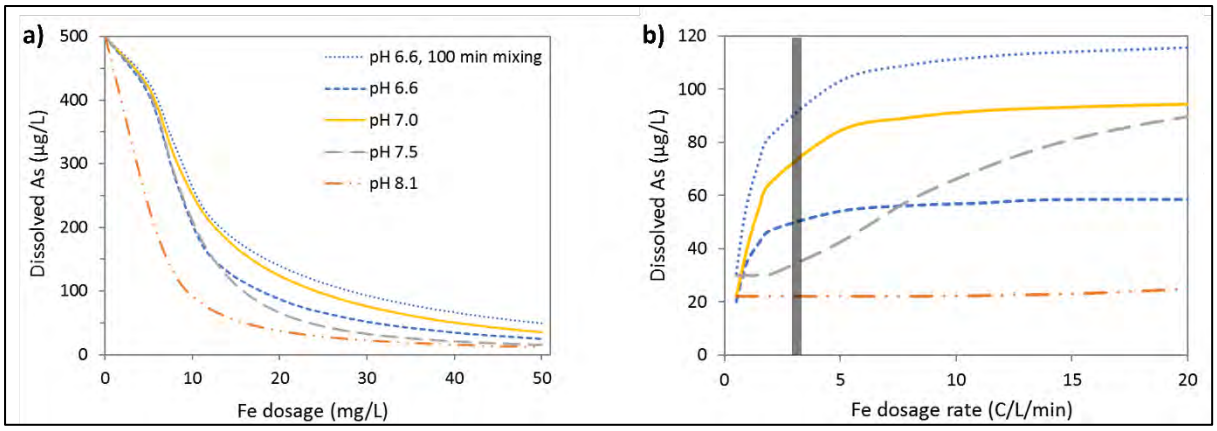

548

549 Figure 3: Post-treatment arsenic concentrations as a function of Fe dosage (panel a, Fe dosage
550 rate of 3 C/L/min) and Fe dosage rate (panel b, Fe dosage of 30 mg/L) according to model
551 simulations at pH 6.6, 7.0, 7.5 and 8.1, assuming O_2 saturation. We report arsenic
552 concentrations at "equilibrium", defined as the time required to reach 99.99% Fe(II) oxidation
553 (300, 100, 10 and 1 min of post-electrolysis mixing at pH 6.6, 7.0, 7.5, and 8.1, respectively).
554 At pH 6.6, post-treatment arsenic concentrations are also given for a more realistic post-
555 electrolysis mixing time of 100 min, at which 99% Fe(II) oxidation is achieved. On panel b, the
556 vertical line at 3 C/L/min indicates the Fe dosage rate used in the simulations presented in
557 Figure 4.

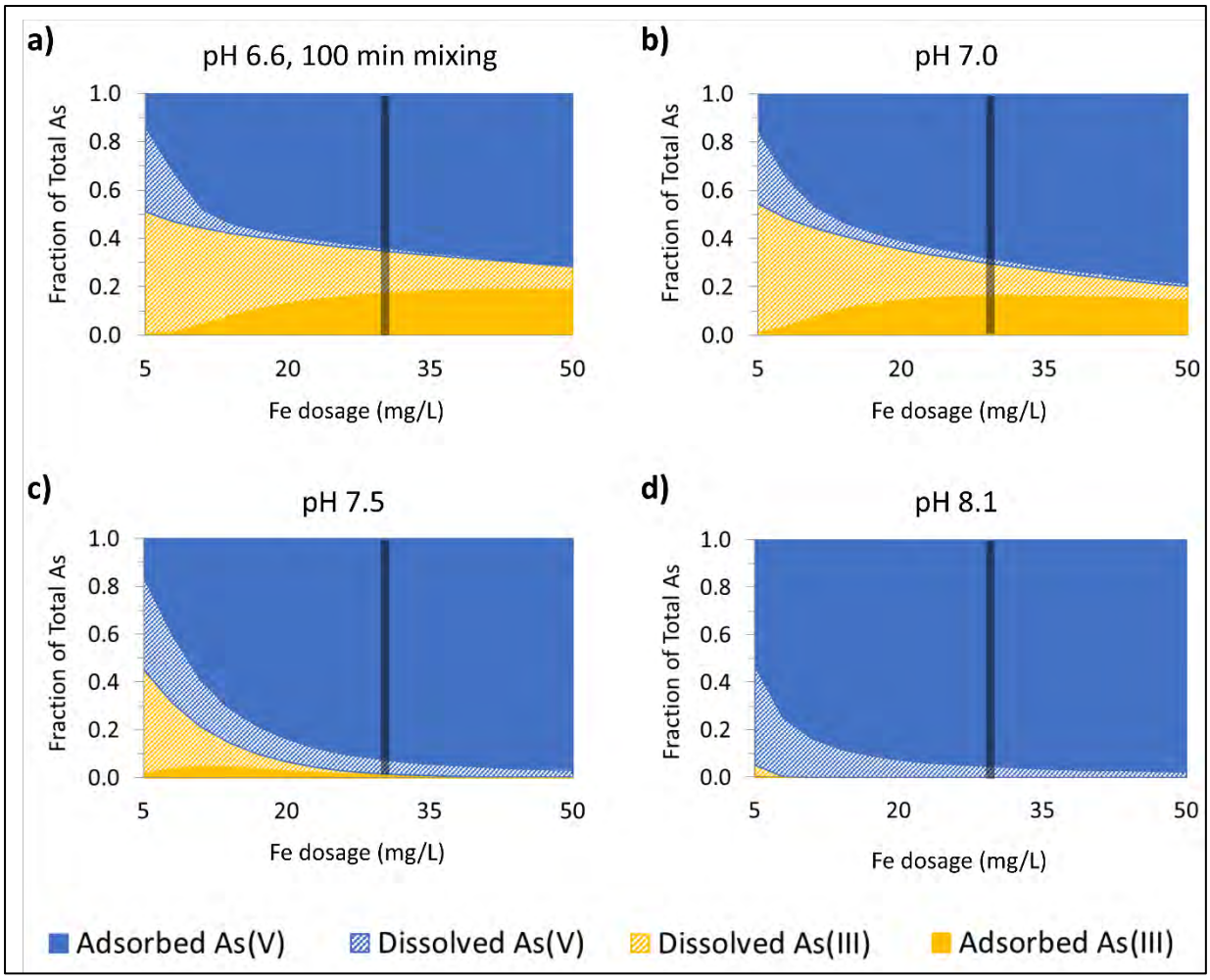

Figure 4: Post-treatment arsenic speciation as a function of Fe dosage according to model simulations assuming O_2 saturation for a Fe dosage rate of 3 C/L/min in four scenarios: pH 6.6 (panel a), 7.0 (panel b), 7.5 (panel c), and 8.1 (panel d). Except for pH 6.6, we report arsenic concentrations "at equilibrium", defined as the time required to reach 99.99% Fe(II) oxidation (100, 10 and 1 min of post-electrolysis mixing at pH 7.0, 7.5, and 8.1, respectively). At pH 6.6, arsenic concentrations are reported for a post-electrolysis mixing time of 100 min, at which 99% Fe(II) oxidation is achieved. On each panel, the vertical line at 30 mg/L indicates the Fe dosage used in the simulations presented in Figure 3b.

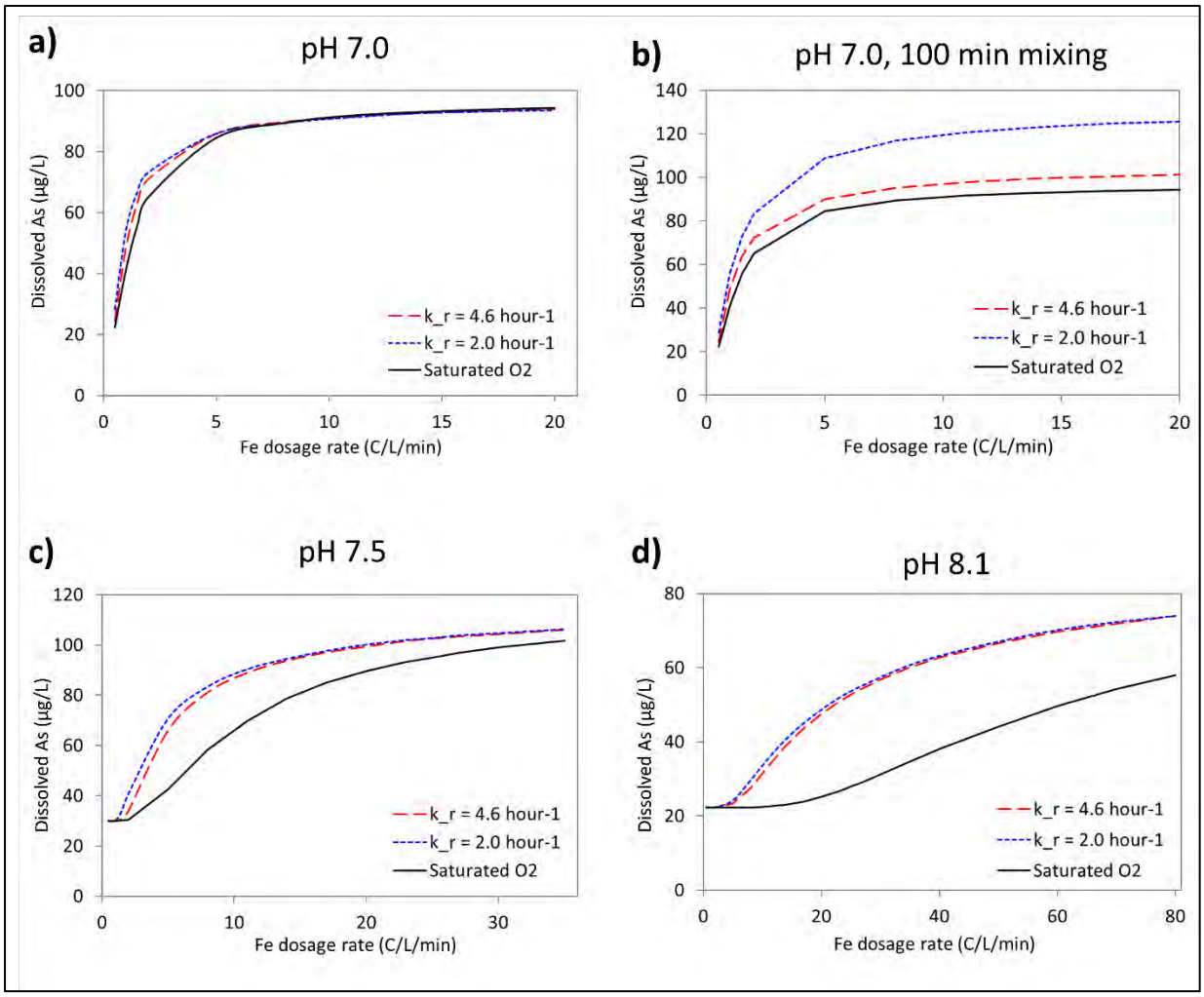

Figure 5: Post-treatment arsenic concentrations as a function of Fe dosage rate according to model simulations in three O_2 recharge scenarios: at pH 7.0 (panels a and b), pH 7.5 (panel c), and pH 8.1 (panel d). We report arsenic concentrations at "equilibrium", defined as the time required to reach 99.99% Fe(II) oxidation (post-electrolysis mixing time up to 250 min for pH 7.0 and up to 100 min for pH 7.5 and 8.1, depending on the O_2 recharge scenario). At pH 7.0, post-treatment arsenic concentrations are also given for a more realistic post-electrolysis mixing time of 100 min, at which 99.8% Fe(II) oxidation is achieved (panel b).

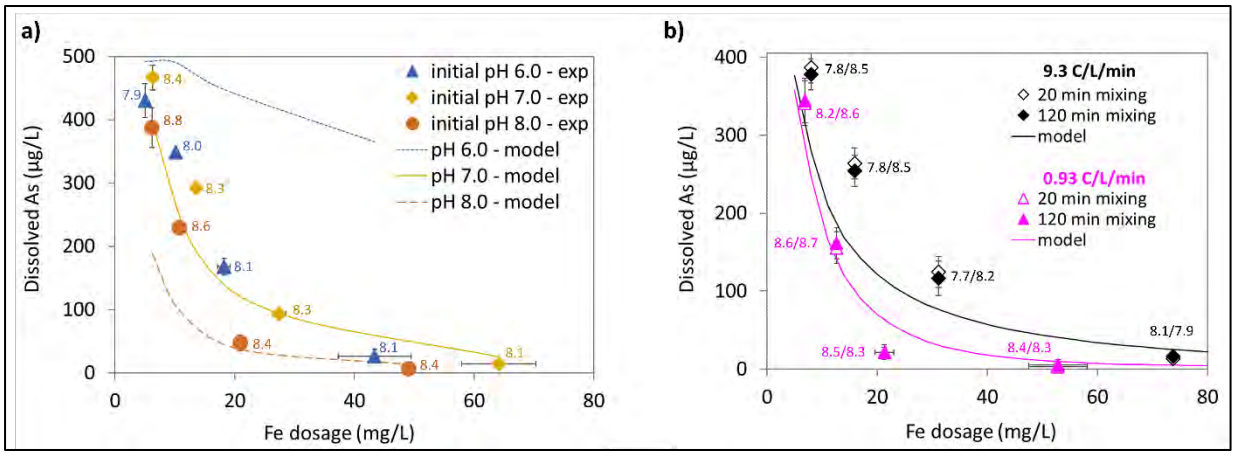

576

577 Figure 6: Post-treatment arsenic concentrations in pH-drift experiments at different initial pH
578 values (panel a, Fe dosage rate of 3.1 C/L/min) and at different Fe dosage rates (panel b, initial
579 pH 7.0). We report averages and standard deviations of duplicate experiments. Post-treatment
580 solution pH is indicated next to the corresponding data point. Model simulations (assuming O_2
581 saturation) are shown (lines) to indicate the expected effect of pH and Fe dosage rate on
582 arsenic removal when pH is held constant.